Structure of the interface between rabbit cortical bone and implants of gold, zirconium and titanium

P. THOMSEN, C. LARSSON, L. E. ERICSON
Institute of Anatomy and Cell Biology, Göteborg University, Medicinaregatan 3, S-413 90 Göteborg, Sweden
L. SENNERBY
Department of Handicap Research, Göteborg University, Göteborg, Sweden
J. LAUSMAA, B. KASEMO
Department of Applied Physics, Chalmers University of Technology, Göteborg, Sweden

The role of surface properties (chemical and structural) for the interaction between biomaterials and tissue is not yet understood. In the present study, implants made of titanium, zirconium (transition metals with surface oxides) and gold (metallic surface) were inserted into the rabbit tibia. Light microscopic (LM) morphometry showed that after 1 and 6 mo the gold implants had less amount of bone within the threads and a lower degree of bone-implant contact than the titanium and zirconium implants, which did not differ from each other. These quantitative differences were supported by LM and ultrastructural observations of the interface. The ultrastructural observations in addition demonstrated that the layer of non-collagenous amorphous material located between the implant and the calcified bone was appreciably thicker around zirconium than around titanium implants. The factors potentially responsible for the observed morphological differences in the bone around the different material surfaces are discussed.

1. Introduction

It is widely accepted that surface properties play an important role in the interaction between implanted materials and tissue [1–3]. However, the specific surface properties of importance are largely unknown. Research aimed at finding correlations between different surface properties and biological responses in different biological systems is required to understand, and eventually to control, material–tissue interactions. The choice of materials in such studies should include variations of surface properties at different controllable levels, ranging from surfaces of different classes of materials (polymers, ceramics, metals), of different materials within one single class (e.g. different metals), and surface modifications of a single material. Surface modifications can include variations of surface structure and/or composition. In previous work we have studied the tissue response to polymers as compared to machined titanium [4] and we are currently also studying tissue responses to different modified titanium surfaces [5]. In the present work, we chose to study the bone response to three different metals, namely titanium (Ti), zirconium (Zr) and gold (Au). The motivation for choosing these materials were that: (i) titanium is a well-known implant material that has been widely and successfully used in several different biomedical applications [6–8]. It is therefore a valuable reference material for this type of study; (ii) zirconium is not widely used as a clinical material, but it is chemically closely related to, and has several properties in common with, titanium. For example, both are transition metals with similar outer shell valence electron structure, and they are normally covered by thin, chemically stable surface oxides. However, most physical and chemical properties, such as oxidation rates, crystal structures, transport properties, water interactions, etc., of the two metals and/or their oxides differ quantitatively [9–11]. It is therefore of interest to investigate whether these different properties influence the biological response; (iii) gold is distinctly different from the other two metals. It is a noble metal which does not form surface oxides (except under extreme conditions). Thus, it exposes a real metallic surface towards the biological environment, in contrast to titanium and zirconium which expose oxide (i.e. ceramic) surfaces [1]. The surfaces of all three materials have in common that they are chemically very stable and highly corrosion resistant in most environments [12], and therefore products released from the implants probably do not influence the biological response.

In this work we show, by light microscopic morphometry and ultrastructural transmission electron microscopy of the implant–tissue interface, that the

0957–4530

above mentioned similarities and differences in surface characteristics between the three materials are indeed reflected in the bone tissue response in the rabbit tibia.

2. Materials and methods

2.1. Implant preparation

Twelve screw-shaped implants (diameter 3.75 mm, length 4 mm) were prepared by machining, from each of the following three materials (all obtained from Edstraco, Stockholm, Sweden); pure gold, zirconium (grade 702, $> 99.2\%$), and titanium (99.7%). All implants were ultrasonically cleaned in successive baths of trichloroethylene, acetone, deionized ($> 18\,\mathrm{MW\ cm^{-1}}$) and sterile-filtered water, and methanol ($10 + 5 + 5 + 5$ min). The ultrasonically cleaned implants were dried in warm ($< 100\,^{\circ}\mathrm{C}$) air.

After the ultrasonic cleaning step, the samples were dry-heat sterilized and ultraviolet (UV)/ozone cleaned [13] in a specially designed vacuum glass cell (Fig. 1) according to the following sequence. Before sample introduction the UV/ozone sterilizing cell was first ultrasonically cleaned in methanol for 15 min, then sealed and evacuated to vacuum (10^{-3} mbar range) under heating, with a mechanical pump. After cool-down, the cell was filled with synthetic air, and opened to air for sample introduction. The samples were placed in the cell, which was once again sealed and evacuated. The cell was flushed with synthetic air three times and then evacuated, first with a mechanical pump and then with a liquid-nitrogen cooled sorption pump. The pressure after 30 min of pumping was less than 1×10^{-3} mbar. This sequence was carried out in order to obtain conditions as clean as possible inside the vacuum cell.

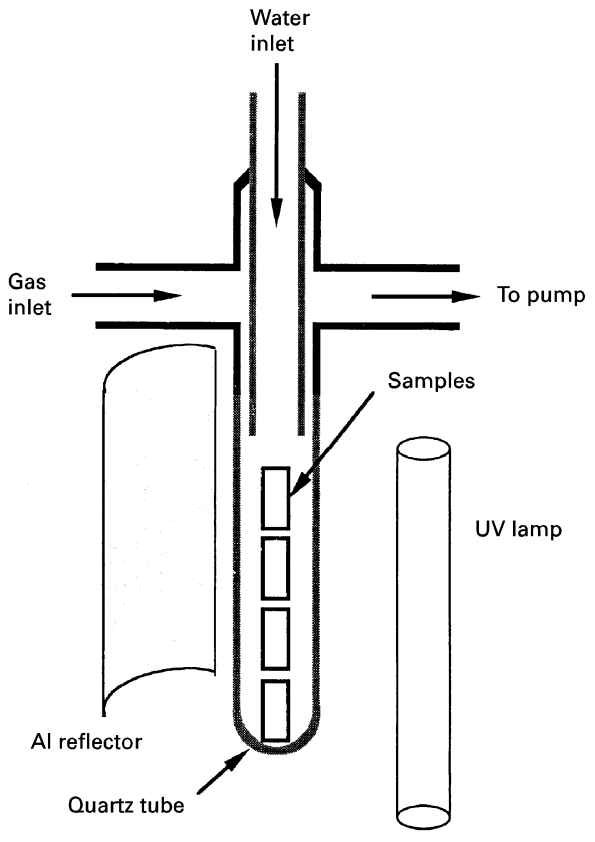

Figure 1 Schematic illustration of the vacuum glass cell for UV/ozone cleaning.

Sterilization of the samples was carried out by filling the cell with synthetic air to 1.5 bar, and heating it to 200 °C for 45 min (i.e. dry-heat sterilization). After cool-down, the samples were irradiated *in situ* by a mercury discharge lamp (main wavelength 254 nm) for 30 min, in order to achieve a final cleaning step which decreased the amount of hydrocarbon contamination at the implant surfaces [13]. After UV/ozone cleaning, the samples were submerged in deionized, sterile-filtered water which was injected into the cell without intervening air exposure. The submerged samples were then transferred into ultrasonically cleaned and dry-heat sterilized glass beakers filled with deionized and sterile-filtered water. The beakers were covered with lids and stored in a laminar air-flow box for a maximum of 24 h before the implants were used. Upon surgery, air exposure of the implant surfaces was prevented by transferring the samples from the sterile water to the implantation site, while maintaining a liquid wetting film on the surface.

2.2. Surface characterization

Implant samples were analysed in a scanning Auger microprobe (SAM, Phi 600, Perkin–Elmer, USA), with facilities for scanning electron microscopy (SEM) and surface-sensitive elemental analysis by Auger electron spectroscopy (AES). The samples were, in most cases (see below), analysed after the ultrasonic cleaning step, i.e. prior to the sterilizing and UV/ozone cleaning procedures. Screw-shaped implants of titanium and zirconium were analysed (two of each). One gold sample, which was not screw shaped but prepared in an identical way to the screw-shaped implants, was analysed.

In order to evaluate the influence of the sterilization, UV/ozone and water-immersion steps, two titanium samples which had gone through the complete preparation sequence, including the final water immersion, were analysed for comparison. These samples were transferred from the water into the introduction lock of the analysis instrument, with a wetting film covering the surface. The wetting film spontaneously disappeared by evaporation when the sample introduction lock was pumped down to vacuum. This procedure prevented the samples from being exposed to ambient air prior to analysis.

SEM was used in the secondary electron mode to evaluate the surface topography and roughness of the three implant materials. AES survey spectra (30–1530 eV) were recorded from areas of $\sim 200\ \mu\mathrm{m}$ diameter in order to detect the elements present at the surfaces. The relative concentrations of the detected elements were estimated from their peak-to-peak heights in the differentiated survey spectra, after correction by tabulated sensitivity factors [14]. This procedure gives the relative concentrations of the detected elements, averaged over the detection volume (typically the three to ten outermost atomic layers), but does not take into account the depth distribution of

the elements. Thus, as is normally the case in AES analysis, the quoted quantitative concentrations must be regarded with some caution. (For details, see the specialized literature on AES analysis, e.g. [15, 16] and references therein.) The electron-beam voltage and beam current during AES analysis were 5.0 keV and 1 μA, respectively. The base pressure in the analysis chamber was typically 5×10^{-9} mbar during AES analysis.

2.3. Animals and surgical procedure

Six adult New Zealand white rabbits of both sexes weighing 4–5 kg were used. The rabbits were anaesthetized by intramuscular (i.m.) injections of fluanison and phentanyl (Hypnorm®, Jenssen, Brussels, Belgium, 0.7 ml/kg body weight) and diazepam (Stesolid®, Dumex, Copenhagen, Denmark, 1.5 mg/kg body weight). Surgery was performed under aseptic conditions. Each tibial metaphysis was exposed with a skin incision and a periosteal flap was raised. Using a drilling-equipment, a hole (1.8 mm diameter) was drilled with low speed (2500 r.p.m.) and subsequently enlarged using larger drills under generous irrigation with saline. After tapping at low speed (16 r.p.m.), the implant was inserted with a screwdriver and placed in level with the cortical bone. Three implants (one of each material) were inserted, 5 mm apart, in each tibia. The location of each type of material varied in a predetermined manner. The periosteum and fascia were sutured with resorbable Vicryl® 5–0 and the skin was closed by silk 3–0 sutures. Post-operatively, the animals were given bensylpenicillin (Intencillin®, Leo, Helsingborg, Sweden, 2.250.000 IE/5 ml, 0.1 ml/kg body weight) and an analgetic, buprenorphin (Temgesic®, Reckitt and Coleman, USA, 0.05 mg/kg body weight) as single injections. The animals were allowed free post-operative movements.

2.4. Specimen retrieval

After 1 and 6 mo, respectively, the animals were killed with an overdose of pentobarbital (Mebumal®, ACO, Solna, Sweden) and fixed by perfusion via the left heart ventricle with 2.5% glutaraldehyde in 0.05 M sodium cacodylate, pH 7.4. The implants and surrounding tissue were removed *en bloc* by sawing and further fixed by immersion in glutaraldehyde. After dehydration in a graded series of ethanol, the specimens were embedded in plastic resin (LR White, The London Resin Co. Ltd, Hampshire, UK). After polymerization, the specimens were divided in two halves by sawing longitudinally through the three implants and surrounding bone. One-half of each specimen was used to prepare about 10 μm thick ground sections for light microscopy (LM) [17]. Sections were stained with 1% toluidine blue. The other half of the implant–tissue blocks were used to prepare thin sections for LM and transmission electron microscopy (TEM). Using a fracture technique [18] the metal was separated from the plastic bloc under a dissecting microscope. The remaining tissue was re-embedded in resin and 1 μm sections were cut for light microscopy. Selected areas were cut for TEM and ultrathin sections were stained with uranyl acetate and lead citrate. The ground sections were analysed in a Leitz Microvid equipment connected to an IBM XT computer, allowing measurements to be performed directly in the microscope. The length of direct bone to implant contact and the amount of bone in each thread was measured. The data are presented as percentage bone–implant contact and as percentage of bone area in each thread. The mean values for each thread on the right and left sides of the section and the mean values for the total implant were calculated [19]. Transmission electron microscopy was performed in a Zeiss CEM 902 or in a Philips EM 400.

3. Results

3.1. Surface characterization

Scanning electron micrographs of the three different implants are shown in Fig. 2. The titanium, zirconium and gold implants had qualitatively similar surface topographies. The most prominent features, common to all three implants, were grooves that were oriented in the machining direction and had widths typically in the 1–10 μm range. Some pits and protrusions, mainly of sizes less than 1 μm, could also be observed on the titanium and zirconium samples. Judging from the scanning electron micrographs, the roughness of the different materials followed the order titanium > zirconium > gold, but with relatively small differences.

The results of the AES analyses are summarized in Table I. The spectra from the two titanium samples were quite similar to each other, and dominated by strong titanium, oxygen, carbon and sodium signals. Minor amounts (a few per cent) of calcium, sulfur, chlorine, silicon, tin and zinc were also detected. For the titanium sample, nitrogen was not included in the table, because it is difficult to detect and quantify on titanium due to peak overlap [20, 21]. Also the spectra from the two zirconium samples were similar to each other. They were dominated by zirconium, oxygen, carbon and nitrogen signals, with smaller signals from calcium, sulfur, chlorine, silicon, sodium and tin. The spectrum from the gold sample was dominated by strong carbon, nitrogen and oxygen signals and smaller peaks from sulfur, chlorine, silicon, sodium and tin detected. Only a weak gold signal was detected. Analysis of the two titanium samples that had gone through the sterilizing and UV/ozone steps prior to analysis showed a decrease of carbon levels to 1–20% as compared to non-UV/ozone treated samples; the inorganic impurities were about the same as in the samples that had only been ultrasonically cleaned.

3.2. Light microscopy

Previous studies in our laboratory [19, 22, 23] have shown that the implantation site in the proximal tibia almost exclusively consists of cortical bone. After implantation, the one or two most proximal threads are located within the cortex, while the remaining part of the screw is protruding into the marrow cavity without

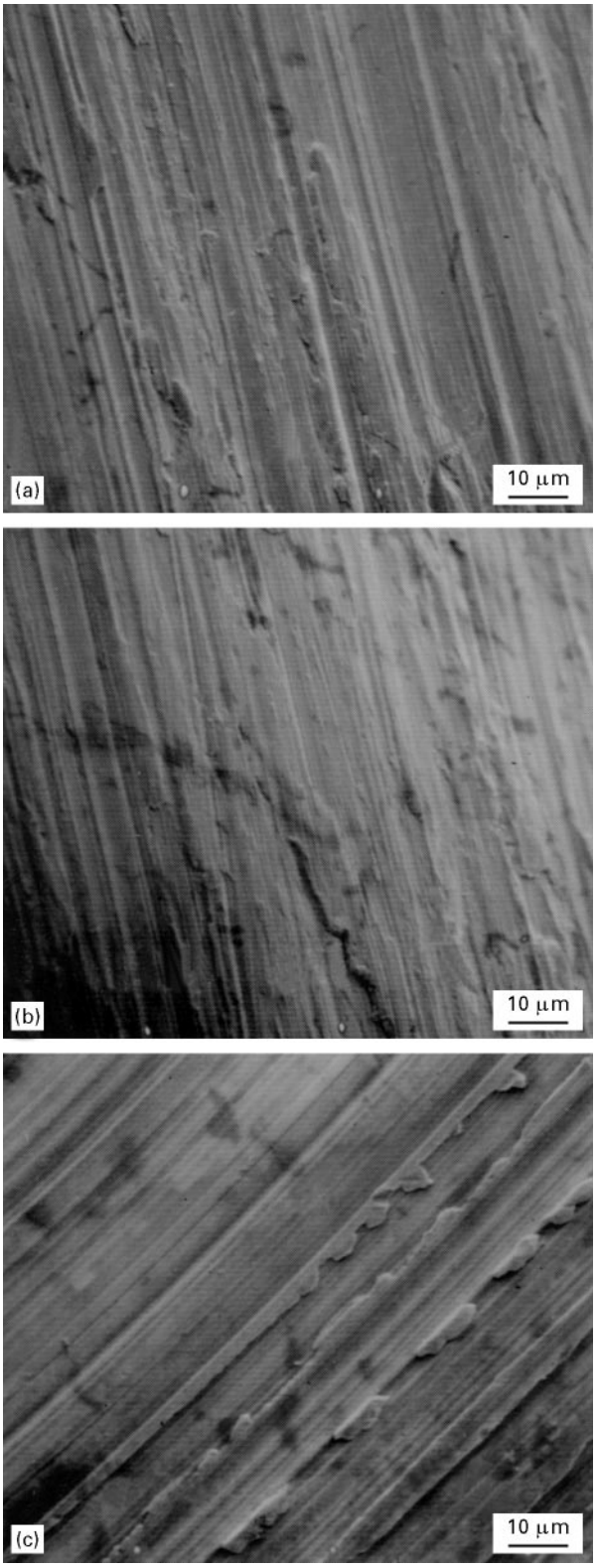

Figure 2 Scanning electron micrographs of implant surfaces: (a) titanium; (b) zirconium; (c) gold.

being in contact with the endosteal surface of the cortex of the opposite side.

At 1 mo, the threads located in the cortex were, to a large extent, filled with new bone which had an immature, woven character, often distinctly demarcated from the mature, lamellar bone in the cortex, (Fig. 3). A general observation made for titanium and zirconium implants but not for gold implants, was that bone trabeculae extended from the endosteal surface towards and into threads (no. 3–4) originally in contact with the marrow cavity (Fig. 3). In the threads which were originally located within the cortical bone, a direct bone contact was more often observed for titanium and zirconium (Figs 4a, b, and 5b–d) than for gold (Fig. 4c).

A periosteal bone formation (occurring both on top of the implant and in the screw-driver slit) was observed around all three types of implants (Fig. 5a). However, a direct contact between the bone and the surface was not generally observed.

Multinuclear cells of varying size and shape were observed on or close to the surface of all three implant materials in areas with soft tissue (Fig. 5e, f). These cells were more frequent on the surface of gold implants.

After 6 mo the implants were surrounded by compact, lamellar bone (Fig. 6). The bone was often in direct contact with titanium and zirconium implants. In contrast, the gold implants were often separated from bone by soft tissue in threads at all levels, although a direct implant–bone contact was also present (Fig. 7).

3.2.1. Morphometry

The morphometric data on the 1 mo specimens are shown in Figs 8 and 9. In comparison with titanium and zirconium, the amount of bone (bone area) within the threads of gold implants was markedly lower (Fig. 8). This was found in threads at all levels, but was most evident in the distal ones. Also the extent of bone–implant contact was lower for gold than for titanium and zirconium implants (Fig. 9). No differences were found between titanium and zirconium implants.

At 6 mo, about 55% of the titanium and zirconium threads were filled with bone. The amount of bone within the threads of gold implants (Fig. 8) had increased in comparison with that observed after 1 mo but was lower than around titanium and zirconium implants. Also the contact between bone and gold implants was lower than for titanium and zirconium implants (Fig. 9).

3.3. Electron microscopy

For ultrastructural studies of the interface between implant and surrounding bone, sections were cut from the second and third thread. From previous studies [5, 19, 22–24] we know that these threads mainly contained bone formed from the endosteal surface of the cortex. It should be pointed out that the specimens were not osmificated and the tissue preservation therefore not optimal.

For titanium implants, the ultrastructure of the interface tissue was identical to that previously described in detail [23]. In many locations, mineralized bone was separated from the implant by a layer of amorphous material never exceeding 400 nm (0.4 μm) in width. However, it should be pointed out that this layer was absent in many locations along the interface;

TABLE I Relative concentrations (at%) of the elements detected in AES survey analyses of the three different implant materials after ultrasonic cleaning

Sample	Element	Ti (418 eV)	Zr (147 eV)	Au (69 eV)	O	C	Ca	S	Cl	Si (90 eV)	Na	Sn (437 eV)	Zn (59 eV)	N
Titanium	Sample 1	7.0	–	–	39.0	39.2	–	1.3	2.1	1.7	8.0	1.2	0.5	–
	Sample 2	8.8	–	–	44.1	34.5	0.2	0.9	1.2	1.7	6.4	1.2	0.9	–
Zirconium	Sample 1	–	6.5	–	36.7	44.3	0.4	0.6	0.7	0.8	2.6	1.4	–	6.0
	Sample 2	–	6.5	–	37.1	44.0	0.6	0.5	0.9	1.3	2.2	1.4	–	5.5
Gold	Sample 1	–	–	0.1	8.5	70.8	–	1.2	1.2	0.3	2.9	2.0	–	13

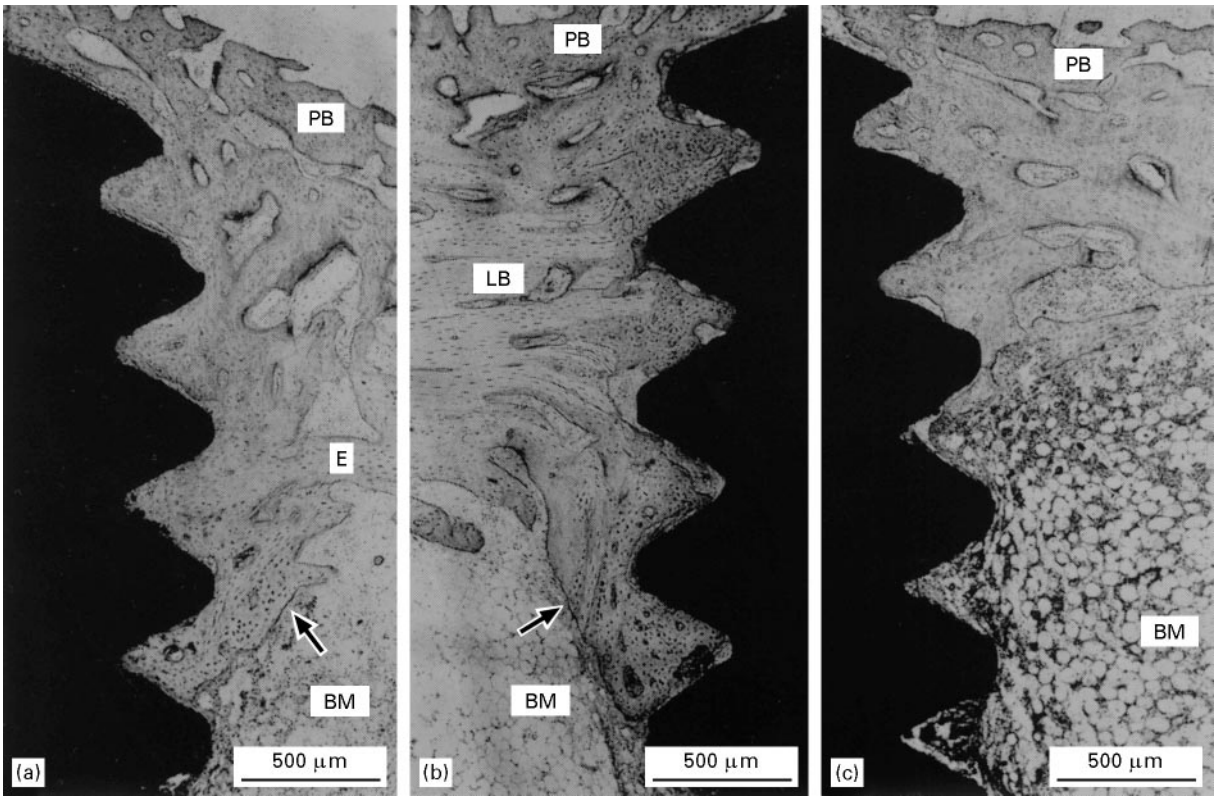

Figure 3 Survey light micrographs of ground sections of implants and surrounding tissue 1 month after insertion. (a) Titanium: bone formation and bone remodelling is observed in the threads and in the surrounding tissue. Periosteal bone formation (PB) and down-growth of trabeculae (arrows) from the endosteal surface (E) is found. BM = bone marrow. (b) Zirconium: as observed for titanium implants, periosteal bone formation (PB) and down-growth from the endosteum (arrows) are evident. The threads are filled with woven bone which is clearly demarcated from the mature, lamellar bone present in the tibia cortex. (c) Gold: periosteal bone formation (PB) is observed. Only the two upper threads located in the cortex are filled with bone. Down-growth of newly formed bone from the endosteal surface (E) is observed. BM = bone marrow.

it is not possible to decide whether this reflects a variable appearance of the amorphous layer or an artefact induced by the separation of the implant from the tissue.

The interface tissue around zirconium implants differed from that around titanium mainly with respect to the width of the amorphous layer, which varied in width from 0.1–0.2 μm (Fig. 10b), up to 4 μm (Fig. 10a–e). Similar to that described for titanium implants [23], in a typical case the amorphous layer had a dense, homogeneous texture. However, it sometimes attained a fibrillar character, probably an effect of insufficient fixation quality (Fig. 10a). Electron-dense deposits containing calcium (verified by imaging EELS) were sometimes present in the amorphous layer (Fig. 10a, c, d). In many areas, mineralized bone reached right up to the amorphous layer (Fig. 10b). In areas where mineralization was lower, a dense line was regularly observed separating bone tissue from the amorphous layer. It is quite possible that such a line is generally present at the border between bone and the amorphous layer but obscured by dense hydroxyapatite crystals when bone mineralization is high. Similar dense lines were present outlining osteocyte canaliculi and were also separating bone of different degrees of mineralization (Fig. 10b). Dense lines in these latter locations have been designated lamina limitans [25]. In several instances, direct continuity between typical laminae limitantes and the dense line at the border between the amorphous layer and bone

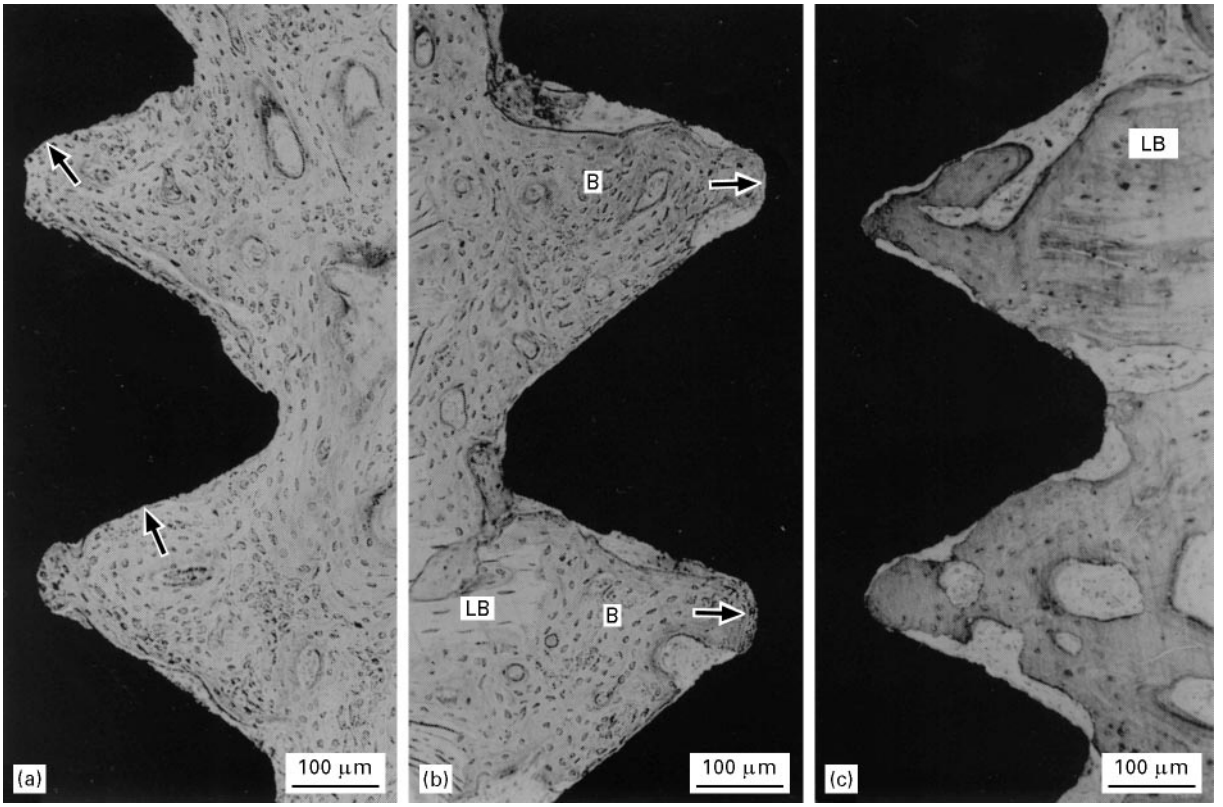

Figure 4 Light micrographs of ground sections of implants and tissue in proximal threads 1 month after insertion. (a) Titanium: the proximal threads contain newly formed bone in contact with the implant surface in several locations (arrows). (b) Zirconium: newly formed bone (B) is located between the mature lamellar bone (LB) and the implant (proximal threads). In several locations the bone is in direct contact with the implant surface, in particular in the bottom of the threads (arrows). In other areas soft tissue is interspersed between the bone and the implant surface. (c) Gold: bone trabeculae are partly occupying the proximal threads. LB = lamellar bone.

tissue was observed. This arrangement with a lamina limitans-like dense line separating the amorphous layer from the bone is also present around titanium implants [23].

In many locations the tissue interfacing with gold implants (Fig. 11a–e), consisted of soft tissue (Fig. 11a, b) with several layers of elongated cells separating the implant from bone tissue. Multinuclear giant cells were often (most commonly after 1 mo after insertion) observed close to the implant surface (Fig. 11a). In other locations, bone tissue was in direct contact with the implant (Fig. 11c–e). It was typical that this bone was not mineralized at all or contained only focal depositions of hydroxyapatite, often concentrated around osteocytes embedded in a dense collagenous matrix (Fig. 11c). The unmineralized collagen matrix was often separated from the implant by a discontinuous (artefacually disrupted during the preparation procedure?) layer of material, not containing collagen fibrils, reminiscent of the material observed adjacent to the surface of titanium and zirconium implants.

4. Discussion

4.1. Implant surface characteristics

The SEM showed that at this resolution level the implants of the three different materials had similar, but not perfectly identical, surface topography. Although no quantitative data are presented here, the scanning electron micrographs indicated that the titanium implants were somewhat rougher than the zirconium implants on the $\sim 1\,\mu m$ scale. The gold implants were the smoothest of the three materials at this resolution level. These small differences in roughness are not unexpected, owing to the differences in hardness and plastic deformation properties, etc., of the materials, which cause variations in the surface topography after machining.

The AES results from the titanium implant surfaces are in line with earlier studies [26–32], and are representative of a surface oxide which is covered by a contamination layer consisting mainly of carbon-containing molecules and some inorganic impurities. It is, however, important to point out here that this surface contamination layer consists of only one molecular monolayer or less of adsorbed molecules (corresponding to ~ 1–$10\,ng$ hydrocarbons per cm^2 surface). This picture of titanium implant surfaces is based on previous extensive analyses of similarly prepared titanium surfaces [26–32], which have shown that they consist of a thin (2–6 nm) surface oxide (mainly TiO_2) covered by one monolayer or less of adsorbed hydrocarbon molecules and smaller amounts of inorganic impurities. The composition of the surface contamination layer, and how it was influenced by the UV/ozone and water-immersion steps on the samples that were actually implanted, is further discussed below.

In analogy with the titanium implants, and taking into account the fact that zirconium, as titanium, is

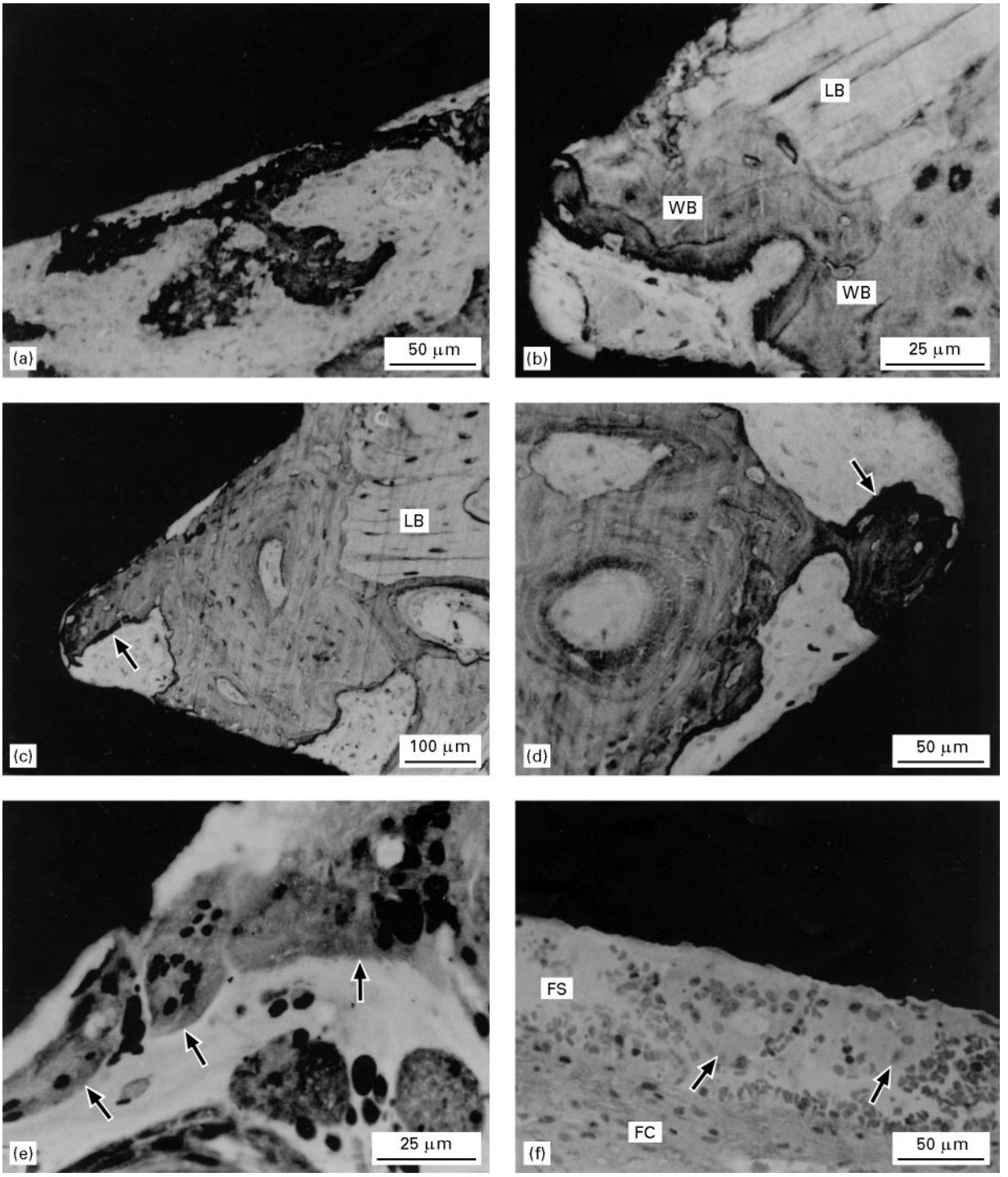

Figure 5 Light micrographs, 1 month after insertion. (a) Periosteal bone formation on top of a titanium implant. No apparent contact between the bone and surface is established. (b) Titanium implant: the edge of mature, lamellar bone (LB) is located in a thread. Woven bone (WB) with several osteocytes is located between the lamellar bone and the surface. A portion of soft tissue is located in the bottom of the thread. (c, d) Zirconium implant: woven bone undergoing remodelling in cortically located threads of a zirconium implant. Both areas with resorption (arrow in c) and with osteoid (arrow in d) are detected. LB = lamellar bone. (e) Distal thread of gold implant. Several multinuclear cells (arrows) are present. (f) Bottom surface of a gold implant. The implant surface is separated from a fibrous capsule (FC) (which in turn is separating the implant from the bone marrow; not shown) by a fluid space (FS). The space contains numerous erythrocytes and is located on the implant surface covered by large, multinuclear cells (arrows).

normally, covered by a surface oxide when exposed to air, we can also interprete the spectra from the zirconium implants as representing a surface oxide covered by a contamination layer. Based on previous studies of oxidized zirconium surfaces [33, 34] and thermodynamical data [11] it is safe to assume that the composition of the oxide in this case is mainly ZrO_2. The position of the Zr_{MNV} Auger peak at 141 eV is also in good agreement with that of bulk ZrO_2 [35] (for metallic zirconium, the MNV peak occurs at 147 eV).

The gold sample, on the other hand, is not expected to be oxidized. In this case, the detected oxygen signal is most likely due to oxygen present in organic molecules in the contamination layer, or to oxygen bound

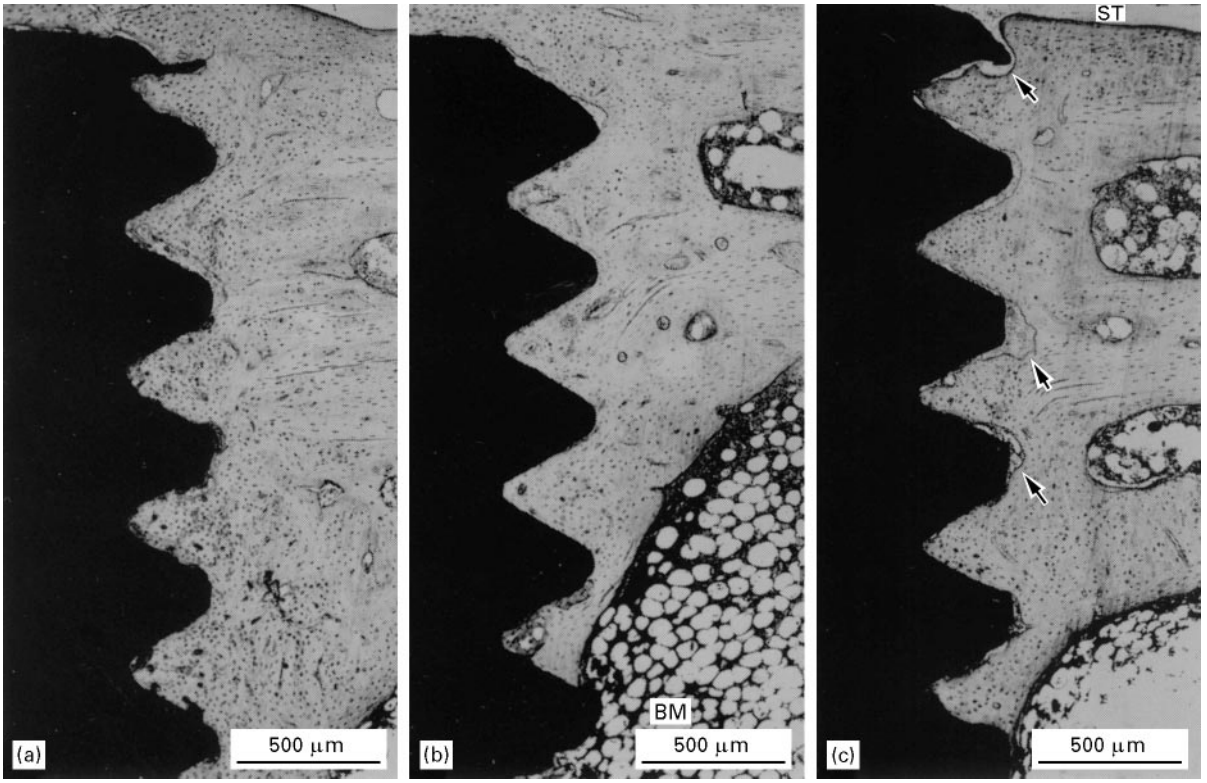

Figure 6 Survey light micrographs of (a) titanium, (b) zirconium, and (c) gold implants and surrounding tissue 6 month after insertion. (a) The top of the titanium implant is covered by bone, in contact with the implant surface. All threads are filled with bone. (b) A zirconium implant which is almost entirely surrounded by bone. BM = bone marrow. (c) A gold implant surrounded by a relatively large amount of bone. The top of the implant is in contact with soft tissues (ST). Several areas with soft tissue are located adjacent to the surface of the threads (arrows).

to the inorganic impurities that were detected. Oxygen in the contamination layer could also explain the high O:Ti and O:Zr ratios for the titanium and zirconium samples, which were significantly higher than those expected for TiO_2 and ZrO_2, respectively. It is also notable how small the gold signal is compared to that of foreign elements (see below).

The fact that the samples were analysed prior to the sterilizing and UV/ozone cleaning step raises the question if the surface compositions are representative of those implants which were actually inserted. The sterilizing and UV/ozone steps and the subsequent evaporation of the water that was used for sample storage prior to analysis, is expected to influence the surface composition of the samples mainly in the following two ways: (i) a significant decrease in the organic contamination levels (due to the oxidative cleaning action of the UV/ozone treatment) [13], and (ii) a possible increase in the amount of inorganic impurities (due to ionic residues from the evaporated water film). The former was confirmed by AES analyses of two titanium samples that had gone through the entire preparation sequence prior to analysis: the carbon levels had decreased to 10%–20%, i.e. a decrease by about a factor of two as compared to the non-UV/ozone treated samples (Lausmaa [36] unpublished results). The inorganic impurities were present in similar or lower concentrations as for the titanium samples that had only been ultrasonically cleaned. Thus, deposition of additional impurities from the water treatment was negligible. These two observations suggest that the surface compositions reported above are fairly representative of the samples which were actually implanted.

It is appropriate and interesting to discuss further the (molecular monolayer of) surface contamination that was detected on the different samples. Carbon contamination is with few exceptions always detected by surface spectroscopy on "practical" surfaces, and is usually assigned to hydrocarbon molecules adsorbed from the ambient air [1, 37]. The amounts of carbon in this contamination layer vary widely depending on the sample type and history. This also applies to inorganic impurities (sodium, silicon, chlorine, sulfur, . . .) which are frequently detected at different implant surfaces [21, 32]. The titanium and zirconium implants analysed here showed relatively similar carbon levels, while the gold sample had a much higher carbon level (before UV/ozone cleaning, see below). When comparing the carbon levels it is important to be aware of the differences in information depth in the AES analysis of the titanium, zirconium and gold samples, respectively (which are due to differences in the kinetic energy of the detected Auger electrons). The significantly lower kinetic energy of the Auger electrons from gold (69 eV) as compared to those of titanium (418 eV) and zirconium (141 eV), means that a given amount of surface contamination attenuates the signals from the underlying gold surface more effectively than for zirconium and titanium. This has the effect of making the analysis more surface sensitive for the gold samples, i.e. it gives rise to apparently

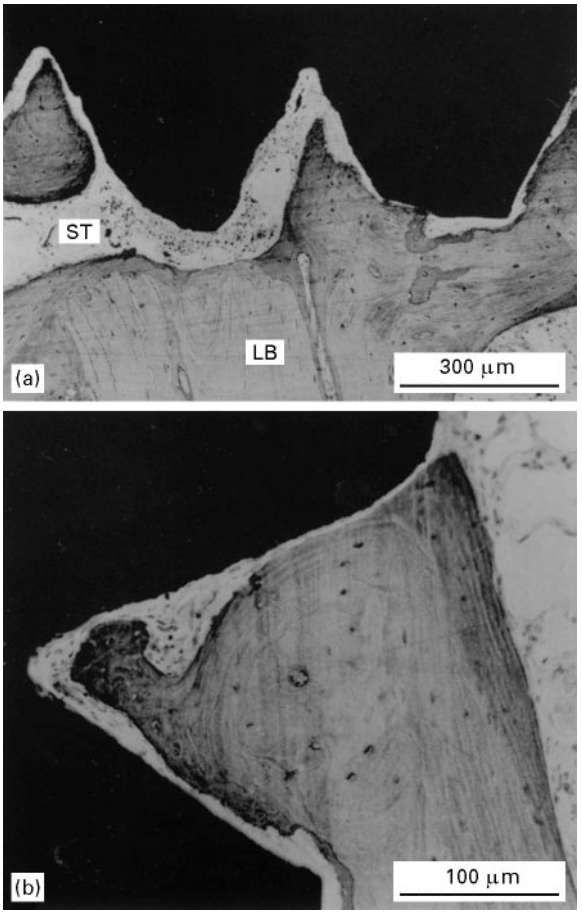

Figure 7 Light micrograph of the tissue surrounding the proximal threads of a gold implant 6 month after insertion. Mature lamellar bone (LB) is separated from the implant surface by soft tissue (ST) which contains inflammatory cells (arrow). (b) Light micrograph of a proximal thread of a gold implant 6 month after insertion. The bone is separated from the implant by soft tissue.

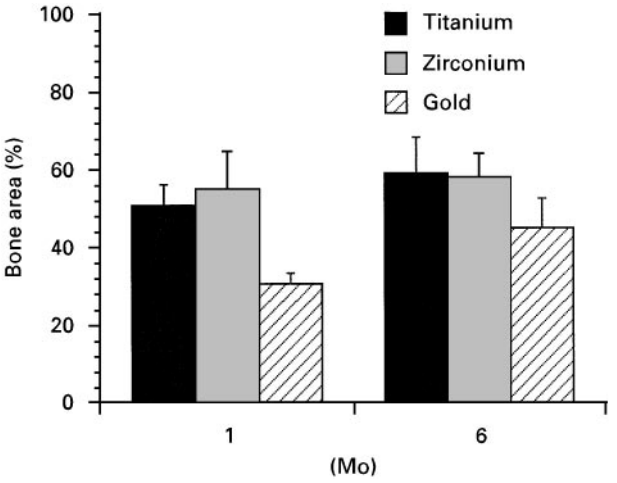

Figure 8 Morphometry. Total bone area (%) after 1 and 6 months, Mean ± S.E.M.

higher surface contamination levels. These differences in surface sensitivity can partly, but not fully, account for the higher carbon level on the gold sample. Because all samples were prepared in a similar way, the observed differences indicate that the gold surfaces had a higher affinity for binding organic molecules

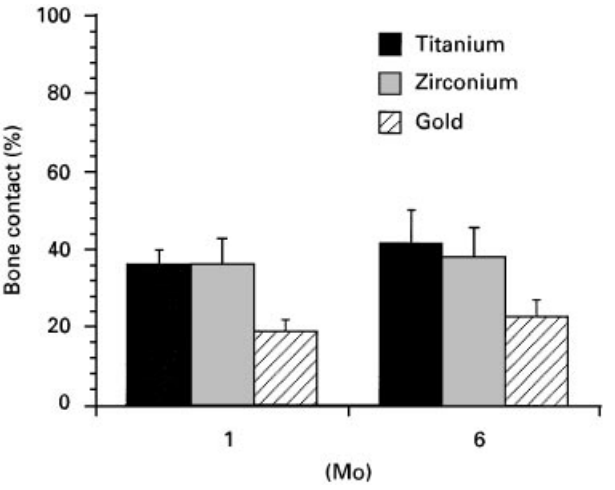

Figure 9 Morphometry. Total bone contact (%) after 1 and 6 months Mean ± S.E.M.

than the other two materials. This is actually not surprising. On titanium and zirconium surfaces, air oxygen helps to saturate the broken surface bonds, by formation of an oxide. On gold this does not occur, leaving a more metallic surface to interact with contaminating hydrocarbons from the air or from cleaning solvents. The amount of inorganic impurities (sulfur, chlorine, silicon, sodium, nitrogen, etc.) was fairly similar for all samples, except for the higher sodium levels detected on the two titanium implants. All of these impurities have previously been detected at different implant surfaces [21, 26–32], with the exception of tin and zinc. The source of the latter two trace impurities was later identified as the methanol which had been used in the final ultrasonic cleaning step.

The fact that the underlying substrates could be detected in all cases, shows that the surface contamination was present as thin overlayers on the molecular monolayer scale and not as real macroscopic films, in qualitative agreement with many previous analyses [5, 20, 21, 26–32].

4.2. Tissue response and relationship to surface characteristics

Major morphological findings in the present study were that the amount of bone within the threads and the degree of bone–implant contact were less for gold implants, as compared to titanium and zirconium. Areas of soft tissues with multinuclear cells and macrophages were also more often observed in association with the gold implants, than with titanium and zirconium. As judged by light and electron microscopy, the morphology around titanium and zirconium implants was similar. However, ultrastructural observations showed that the amorphous layer in contact with zirconium implants was appreciably thicker as compared to titanium; such an amorphous layer was also present in contact with gold implants and in addition, the bone close to these implants was, in general, poorly mineralized.

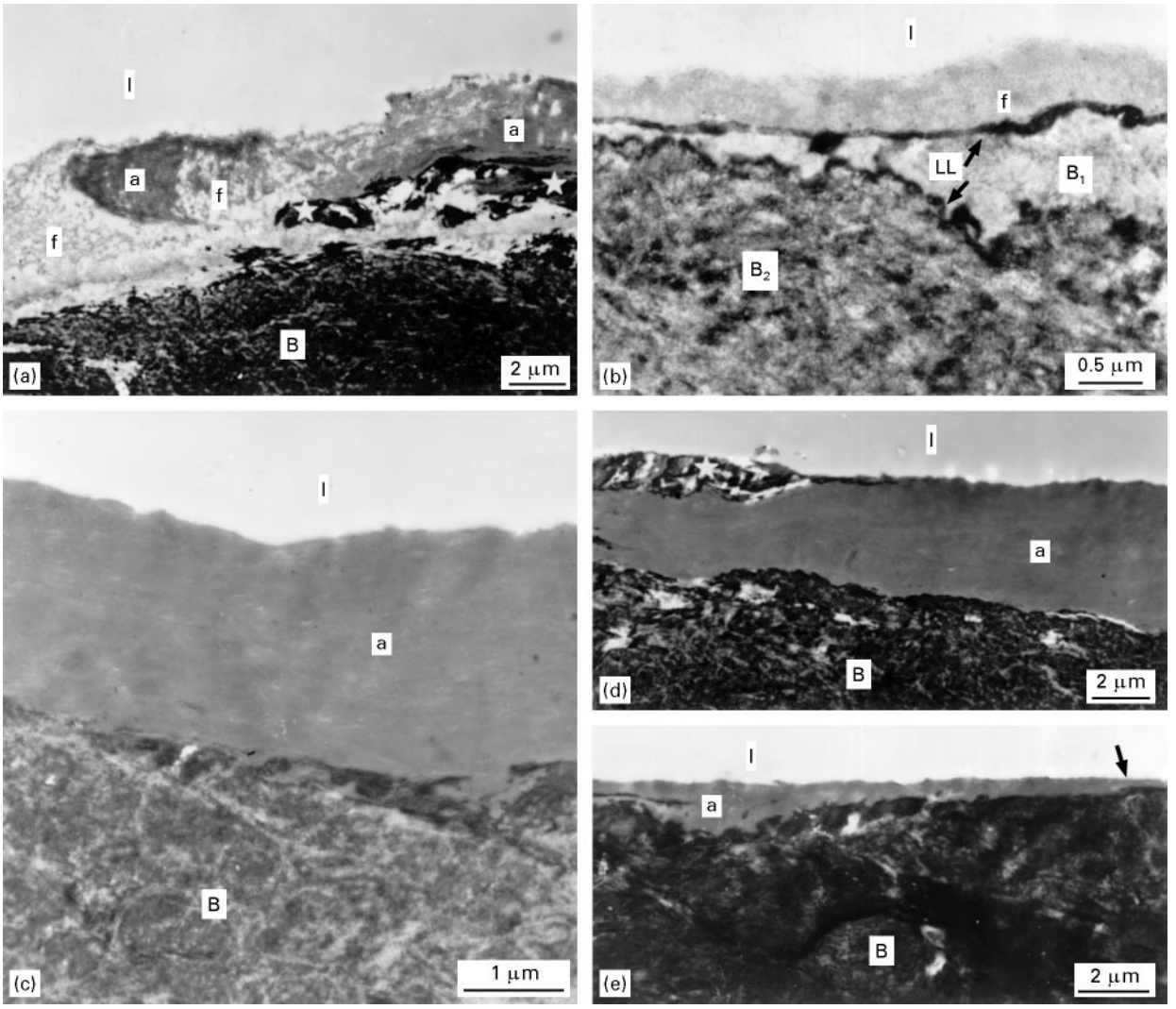

Figure 10 Electron micrographs of tissue adjacent to zirconium implants inserted in the proximal rabbit tibia for 6 months after insertion. Tissue was fixed in glutaraldehyde alone (no osmification step). Sections contrasted with uranyl acetate and lead citrate. Location of the implant (removed by fracture technique) is indicated (I). (a) A 2–3 μm wide layer of non-collagenous material separates the calcified bone tissue (B) from the implant. The material varies in texture from dense amorphous (a) (cf. c, d, e) to loosely fibrillar (f) (cf. b). This variability is probably artefactual related to a non-optimal tissue preservation rather than to a real variation in structure. Electron-dense material, known to contain calcium, is located in the amorphous/fibrillar material outside the calcified bone. (b) Along this portion of the bone–implant interface the material in contact with the implant has a loosely, fibrillar texture (f). A dense lamina limitans-like line (LL) separates the fibrillar material from poorly mineralized bone (B_1). A similar line is also separating the poorly mineralized bone (B_1) from more completely mineralized bone (B_2). (c, d, e) Various aspects of the non-collagenous layer of amorphous material separating mineralized bone (B) from direct contact with the implant. This morphological appearance is the most typical (cf. a, b). The width varies from 3–4 μm (c, d) to 0.1–0.2 μm (arrow in e). The amorphous material often contains deposits of calcium (∗) located close to the bone (a) or close to the implant surface (d).

Comparing these results with earlier studies we find the following: Albrektsson *et al.* [38] have previously compared the bone response to titanium and gold, by using polymer implants that had been sputter coated by thin metal films. While such implants are not representative for implants made by machining of the bulk metal, they still represent the same materials studied with respect to surface chemistry. Albrektson *et al.* observed qualitatively similar differences between gold and titanium as in this work.

Williams [8] compared the adsorption of albumin and other proteins on gold, titanium and other oxide-covered metals. Also at this level, the biological response to gold differed from that to titanium: the gold surfaces were found to adsorb significantly larger amounts of albumin than the titanium oxide surfaces.

Albrektsson *et al.* [39] studied the ultrastructure of bone adjacent to zirconium and titanium sputter-coated polycarbonate plugs (about 100 nm thick coatings) 6 mo after insertion in rabbit bone. The authors did not find soft tissue in the interface, nor any adverse tissue reactions and concluded that both metals were "well accepted". They did, however, consider titanium to have a better biocompatibility than zirconium due to the more "nature-like" thickness of the proteoglycan layer around the titanium implants.

Galante and Rostoker [40] investigated the soft tissue response to Zircalloy (Zr 98%, Sn 1.5%, Fe 0.15%, Cr 0.1%), vitallium, stainless steel, Ti6Al4V and titanium. Twelve months after insertion in rabbit muscle, light microscopy revealed a fibrous capsule formation around all materials. The thickest fibrous

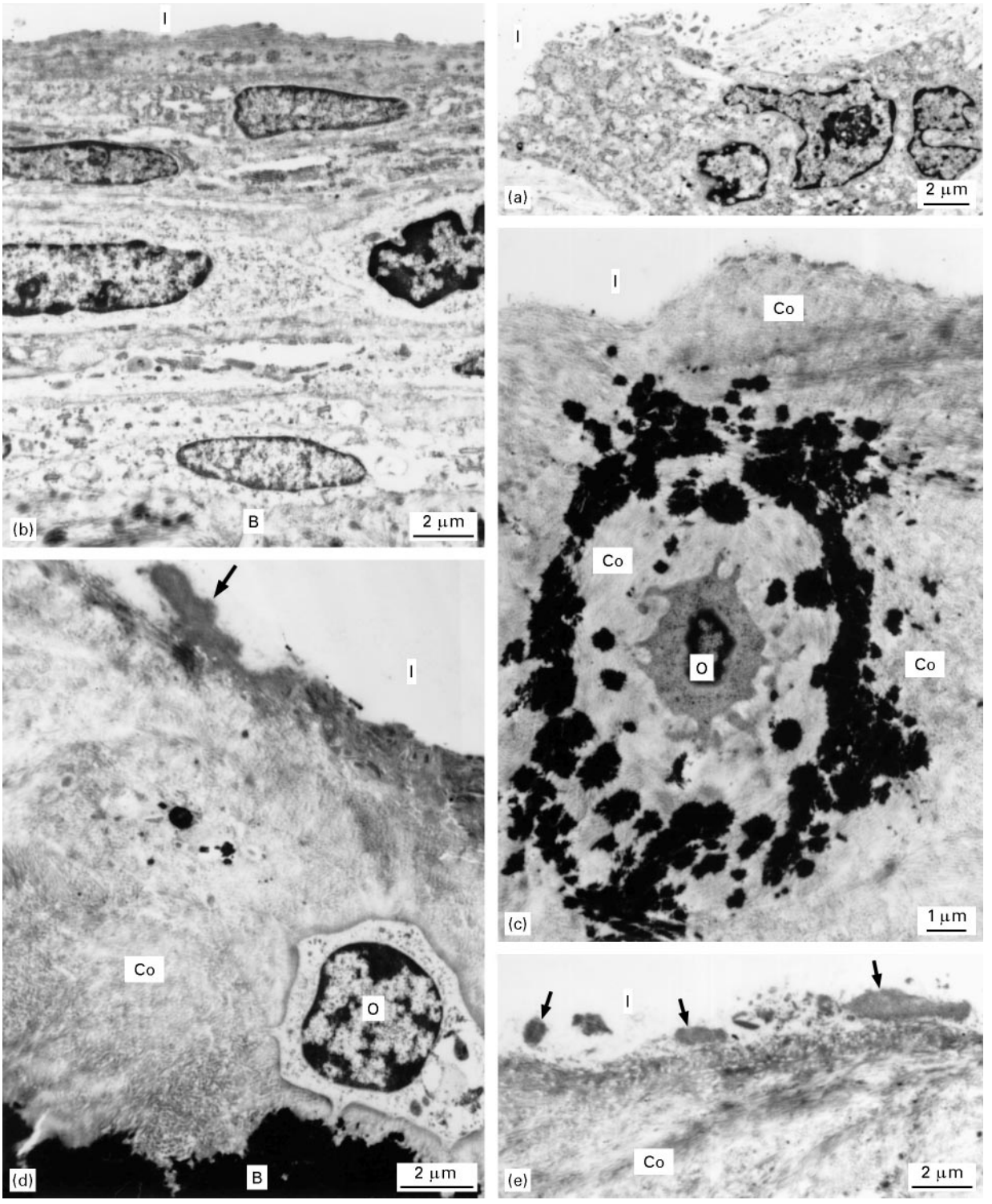

Figure 11 Electron micrographs of tissue adjacent to gold implants inserted in the proximal rabbit tibia for 1 month (a) or 6 months (b–e). Location of removed implant = I. Tissue preparation similar to zirconium implants. (a) Multinuclear giant cell located close to and probably in contact with the implant surface 1 month after insertion. (b) Soft tissue is often present adjacent to gold implants. Elongated cell profiles with elongated nuclear profiles separate the implant from poorly mineralized bone matrix (B). (c) In many locations along the implant–tissue interface, poorly mineralized bone, characterized by a dense collagenous (Co) matrix and embedded osteocytes (O), is present. As exemplified here, focal deposits of hydroxyapatite crystals, typically concentrated around osteocytes, is often observed, while fully mineralized bone close to the implant is uncommon (albeit it may occur). (d) Another example of an osteocyte embedded in an essentially non-mineralized matrix located close to the implant as well as close to fully mineralized bone (B). Dense, partially amorphous, material (arrows), not containing collagen fibrils, form a discontinuous layer adjacent to the implant. Co = collagen. (e) Another example of the discontinuous (disrupted during the preparation procedure?) layer of dense, partially amorphous, material (arrows) located adjacent to the implant and separating it from a dense, non-calcified collagenous (Co) matrix.

membrane was found around zirconium, but the differences were small. In a similar study, Laing *et al.* [41] studied metal implants in rabbit muscle after 6 mo. These authors also found that zirconium had a thicker fibrous capsule than titanium and titanium alloys.

Thus, the morphological findings in this work are in qualitative agreement with other studies in bone.

A key question is then: are the observed differences in the bone response to gold and zirconium/titanium respectively due to differences in: (i) the intrinsic surface properties and/or (ii) the surface roughness, and/or (iii) the contamination layers covering the surfaces of the implants. These three different factors are discussed below.

As previously pointed out, titanium and zirconium have several properties in common. They are both transition metals and are found in the same group in the Periodic Table of the elements, which means that they have similar outer shell valence electron structures. Owing to their reactivity with oxygen, these metals are normally covered by surface oxides, i.e. they expose surfaces that are ceramic rather than metallic. Their most common surface oxides, TiO_2 and ZrO_2, respectively, have quite similar thermodynamical properties [11]. With regard to their interaction with many simple molecules, both TiO_2 and ZrO_2, can be classified as relatively active materials. For example, both are catalytically active in a number of organic reactions [11, 42], and they can both dissociate water molecules upon adsorption to form hydroxyl groups at their surfaces [43]. On the other hand, both TiO_2 and ZrO_2 are quite stable in aqueous solutions and the pH's that normally prevail *in vivo* [12]. Both titanium and zirconium are therefore expected to be relatively corrosion resistant *in vivo*. Thus the surface properties of the two materials are qualitatively similar in many respects, although most of the physical and chemical properties mentioned above, differ quantitatively.

Gold, on the other hand, is a noble metal which is normally metallic and oxidized only under extreme oxidizing conditions. It therefore presents a metallic surface towards the biological surroundings. From a global chemical point of view, gold is very inactive. For example, it is normally not catalytically active and generally does not dissociate molecules upon adsorption. Gold is also highly corrosion resistant under physiological conditions [12]. However, on the monolayer scale, gold can exert considerable bonding strength on molecules, mainly through its high polarizability as a metal. The latter is the likely mechanism behind the bonding of the contamination layer.

The second point above, concerning surface roughness, can be discussed with reference to studies of the influence of surface roughness on tissue response [44–51]. It has been shown that surface roughness on the ~ 10 μm scale influences both tissue responses *in vivo* and cellular responses *in vitro*. The three groups of implants studied in this work had quite similar surface topographies on this scale. The influence of surface roughness at the level of ~ 1 μm and smaller on the bone response *in vivo* has, however, not yet been systematically studied. Because the present implants showed some differences in surface roughness at this level, especially gold versus the other two materials, it cannot be excluded that this may have contributed to the different bone morphologies observed.

The third and final subject, namely the potential influence of (sub)monolayer surface contamination on the tissue response, is essentially an open question which has not yet been addressed by systematic studies. We consider it unlikely that the low absolute amounts (~ 1–10 ng cm^{-2} implant surface) of impurities, and the relatively small differences that were observed between the implants in this respect, could have been a major factor influencing the observed differences in bone response, especially because both the absolute carbon concentrations and the difference between them was probably diminished after the UV/ozone cleaning step, which has a well-documented effect of decreasing organic surface contamination at surfaces [13].

In view of the overall surface characteristics of the materials studied here, it is thus most likely that the observed differences in bone response were caused by differences in intrinsic surface properties between the materials. With respect to surface properties, gold is very different from zirconium and titanium (oxides), while the latter two are quite similar to each other. This is consistent with the observation that the gold implants caused a distinctly different bone response from the titanium (oxide) and zirconium (oxide) implants, while the latter two caused qualitatively similar bone responses. (Note that the difference between gold on the one hand, and titanium and zirconium, on the other, may have been partly masked by the contamination layers, i.e. the difference may be amplified if perfectly clean surfaces could be used.)

The results suggest that the titanium and zirconium oxides have a positive effect on the tissue–material interaction, or alternatively, that gold has a negative effect. Whether the observed differences in bone response originate from a positive effect by TiO_2 and ZrO_2, or a negative effect by gold is a question of major interest.

5. Conclusion

Distinctly different bone responses were observed between implants of gold on the one hand, and implants of titanium and zirconium, on the other. Gold induced significantly less bone formation around the implants and soft tissue formation was more frequently observed, as compared to implants of titanium and zirconium. Titanium and zirconium gave rise to similar amounts of bone around the implants, but differences could be detected at the ultrastructural level. The observed differences in bone response are consistent with the known similarities and differences in physical and chemical surface properties between the three studied materials.

Acknowledgements

This study was supported by the Swedish National Association against Rheumatism, the King Gustaf V 80-year Fund, the Swedish National Board for Industrial and Technical Development NUTEK and the Swedish Medical Research Council (9495). Part of this work was carried out within the Swedish Biomaterial Consortium, funded by NUTEK and the Swedish Natural Science Research Council. We wish to thank Lena Emanuelsson and Gunnel Bokhede for expert technical assistance.

References

1. B. KASEMO and J. LAUSMAA, *CRC Crit Rev. Biocomp.* **2** (1986) 335.
2. B. D. RATNER, *J. Biomed. Mater. Res.* **27** (1993) 837.
3. R. E. BAIER, A. E. MEYER and J. R. NATIELLA, in "Tissue integration in oral, orthopedic and maxillofacial reconstruction", edited by D. E. T. W. R. Laney. (Quintessence, Chicago, 1992) pp. 240–9.
4. P. THOMSEN, L. M. BJURSTEN and L. E. ERICSON, *Scand. J. Plast. Reconstr. Surg.* **20** (1986) 173.
5. C. LARSSON, P. THOMSEN, J. LAUSMAA, M. RODAHL, B. KASEMO, and L. E. ERICSON, *Biomater.* **15** (1994) 1062.
6. R. ADELL, U. LEKHOLM, P.-I. BRÅNEMARK, and T. JEMT, *Int. J. Oral Maxillofac. Implants* **5** (1990) 347.
7. P.-I. BRÅNEMARK, G. A. ZARB and T. ALBREKTSSON, "Tissue integrated prostheses: Osseointegration in clinical practice." (Quintessence, Chicago, 1985).
8. D. F. WILLIAMS, *J. Med. Eng. Technol.* **1** (1977) 266.
9. V. E. HEINRICH, "The surface science of metal oxides" (Cambridge University Press, Cambridge, 1994).
10. J. F. KENNEDY and J. M. S. CABRAL, *Transit. Met. Chem.* **11** (1986) 41.
11. G. V. SAMSONOV, "The oxide handbook" (IFI/Plenum, New York, 1973).
12. M. POURBAIX, "Atlas of electrochemical equilibria" (National Association of Corrosion Engineers, Huston, 1966).
13. J. R. VIG, *J. Vac. Sci. Technol.* **A 3** (1985) 1027.
14. L. E. DAVIS, N. C. MACDONALD, P. W. PALMBERG, G. E. RIACH and R. E. WEBER, "Handbook of Auger electron spectroscopy." (Physical Electronics, Eden Prairie, 1978) pp. 5–18.
15. C. R. BRUNDLE and A. D. BAKER, "Electron spectroscopy: theory, techniques and applications". (Academic Press, London, 1981).
16. D. BRIGGS and M. P. SEAH, "Practical surface analysis. Auger and X-ray electron spectroscopy", Vol. 1 (Wiley, Chichester, 1990).
17. K. DONATH and G. A. BREUNER, *J. Oral Pathol.* **11** (1982) 318.
18. P. THOMSEN and L. E. ERICSON, *Biomater.* **6** (1985) 421.
19. L. SENNERBY, P. THOMSEN and L. E. ERICSON, *Int. J. Oral. Maxillofac. Impl.* **7** (1992) 62.
20. J. LAUSMAA, T. RÖSTLUND and H. McKELLOP, *Surf. Interface Anal.* **15** (1990) 328.
21. J. LAUSMAA, B. KASEMO and H. MATTSSON, *Appl. Surf. Sci.* **44** (1990) 133.
22. L. SENNERBY, P. THOMSEN and L. E. ERICSON, *J. Mater. Sci. Mater. Med.* **4** (1993) 240.
23. *Idem., ibid.* **4** (1993) 494.
24. C. LARSSON, P. THOMSEN B.-O. ARONSSON, M. RODAHL, J. LAUSMAA, B. KASEMO and L. E. ERICSON, *Biomater.* **17** (1996) 605.
25. J. P. SCHERFT, *J. Ultrastruct. Res.* **64** (1978) 173.
26. P. P. BINON, D. J. WEIR and S. J. MARSHALL, *Int. J. Oral Maxillofac. Impl.* **7** (1992) 168.
27. J. H. DUONDUOLAKIS, *J. Prosthet. Dent.* **58** (1987) 417.
28. J. A. GARDELLA Jr., T. G. VARGO, T. J. HOOK, G. L. GROOBE III, L. SALVATI Jr and J. HAUTANIEMI, in "Surface characterization of biomaterials," edited by B. D. Ratner (Elsevier, New York, 1988) pp. 149–60.
29. J. LAUSMAA, L. MATTSSON, U. ROLANDER and B. KASEMO, in "Biomedical materials", edited by M. F. N. J. M. Williams and W. Zingg (Materials Research Society, Pittsburgh, 1986) pp. 351–9.
30. J. LAUSMAA, B. KASEMO, U. ROLANDER, L. M. BJURSTEN, L. E. ERICSON, L. ROSANDER and P. THOMSEN, in "Surface characterization of biomaterials", edited by B. D. Ratner, (Elsevier, New York, 1988) pp. 161–74.
31. J. LAUSMAA, 'Surface oxides on titanium: Preparation, characterization and biomaterial properties", (University of Gothenburg, Gothenburg, 1991).
32. D. C. SMITH, R. M. PILLIAR, J. B. METSON and N. S. McINTYRE, *J. Biomed. Mater. Res.* **25** (1991) 1069.
33. K.-O. AXELSSON, K.-E. KECK and B. KASEMO, *Surf. Sci.* **164** (1985) 109.
34. P. PRIETO, L. GALÁN, J. M. SANZ and F. RUEDA, *Surf. Interface Anal* **16** (1990) 535.
35. K.-O. AXELSSON, K.-E. KECK and B. KASEMO, *Surf. Sci.* **25** (1986) 217.
36. J. LAUSMAA, unpublished results.
37. B. KASEMO and J. LAUSMAA, *J. Biomed. Mater. Res.* **22** (1988) 145.
38. T. ALBREKTSSON, P.-I. BRÅNEMARK, H.-A. HANSSON, B. IVARSSON and U. JÖNSSON, in "Clinical applications of biomaterials," edited by T. A. A. J. C. Lee and P.-I. Brånemark, (Wiley, New York, 1982) pp. 167–77.
39. T. ALBREKTSSON, H.-A. HANSSON and B. IVARSSON, *Biomater.* **6** (1985) 97.
40. J. GALANTE and W. ROSTOKER, *Clin. Orthop. Rel. Res.* **86** (1972) 237.
41. P. G. LAING, A. B. FERGUSON and E. S. HODGE, *J. Biomed. Mater. Res.* **1** (1967) 135.
42. H. H. KUNG, "Transition metal oxides: surface chemistry and catalysists", (Elsevier, Amsterdam, 1989).
43. P. A. THIEL and T. E. MADEY, *Surf. Sci. Rept.* **7** (1987) 211.
44. M. HORMIA M. KÖNÖNEN, J. KIVILAHTI, J. HAUTANIEMI and I. THESLEFF, *J. Biomed. Mater. Sci.* **26** (1992) 1325.
45. A. S. G. CURTIS and P. CLARK, *Crit. Rev. Biocomp.* **5** (1990) 344.
46. B. CHEHROUDI, T. R. L. GOULD and D. M. BRUNETTE, *J. Biomed. Mater. Res.* **23** (1989) 1067.
47. *Idem, ibid.* **24** (1990) 1202.
48. D. BUSER, R. K. SCHENK, S. STEINEMANN, J. P. FIORELLINI, C. H. FOX, and H. STICH, *ibid.* **25** (1991) 889.
49. D. M. BRUNETTE, "Surface characterization of biomaterials," edited by B. D. Ratner, (Elsevier, New York, 1988) pp. 203–18.
50. *Idem, Int. J. Oral. Maxillofac. Impl.* **3** (1988) 231.
51. K. T. BOWERS, J. C. KELLER, B. A. RANDOLPH, D. G. WICK, and C. M. MICHAELS, *ibid.* **7** (1992) 302.

Received 12 March
and accepted 4 April 1997